Cent. Eur. J. Geosci. • 4(3) • 2012 • 478-494
DOI: 10.2478/s13533-011-0079-2

VERSITA

Central European Journal of **Geosciences**

Refinement of genetic and structural models of the Úrkút manganese ore deposit (W-Hungary, Europe) using statistical evaluation of archive data

Research Article

Lóránt Bíró[1*], Márta Polgári[2†], Tivadar M. Tóth[1‡], Tamás Vigh[3§]

1 *Department of Mineralogy, Geochemistry and Petrology, University of Szeged, Egyetem u. 2., H-6722 Szeged, Hungary*

2 *Institute for Geochemical Research, HAS, Budaörsi u. 45., H-1112 Budapest, Hungary*

3 *Manganese Mining and Processing Ltd., Külterület 1., H-8409 Úrkút, Hungary*

Received 16 May 2012; accepted 20 July 2012

Abstract: Although the Úrkút manganese ore deposit in western placecountry-regionHungary has been exploited for at least 90 years, there are still numerous open questions concerning ore genetics as well as structure and geometry of the ore body. A large set of available archive data for the deposit have been reviewed and evaluated in order to solve some of the most crucial problems. For processing, besides diverse GIS approaches, univariate and multivariate statistical methods were used on the created unified database. The main aims of the mathematical treatment were giving a classification scheme for the wide spectrum of Mn-ores based on their chemical composition (Mn, Fe, Si, P) as well as evaluation of their spatial distribution. For the ore characterization and understanding the genetic processes, cluster and discriminant function analyses were used. Results of the multivariate treatment verified the existence of different ore types and provided an exact chemical definition for all of them. It alsoinferred that the main geochemical processes that took place in ore genesis were similar for all sample groups (ore types) with significantly different weights in each case.

A 3D evaluation of the Úrkút mine heading map system shows that the ore body covers the footwall surface as a stratiform sheet throughout the study area. Palaeo-relief studies suggest a significant difference between the footwall and hanging wall morphologies which clearly implies tectonic activity following ore deposition. The deposit was affected by an E-W compression stress field near the Aptian-Albian transition causing folding of the Mn deposit.

Keywords: Úrkút • manganese (Mn) • Jurassic • Aptian-Albian • multivariate statistical methods

*E-mail: birolori@gmail.hu
†E-mail: rodokrozit@gmail.com
‡E-mail: mtoth@geo.u-szeged.hu
§E-mail: manganvigh@vnet.hu

1. Introduction

Mining of the manganese ore in the Úrkút area commenced in the early 1920s. During the last 90 years of active exploitation, a large amount of different types of data have been collected. Field and borehole data provide(?) stratigraphic and structural information. Exploration work which covered the entire deposit area produced alarge number of chemical analyses for a few of the most important elements for ranking the manganese ore. To date, this data has only been collated in unpublished research reports summarized by [1]. From the first decades of mining activity, only a few archived samples are available for modern investigations. Consequently, data from the historic mining operations remain the only source of information, due to certain ore types having been entirely exhausted, and early mining areas have already been closed. Both industrial and scientific investigations of the mineralization have been in progress in the past decades. Small portions of the deposit were subjected to detailed studies, with the goal of characterizing the ore and its conditions of formation [2]. Recently, a new genetic model was proposed for the Mn deposit according to which two cycles of bacterial activity took place during ore formation. Cycle 1 was a near-seabed aerobic chemolithoautotroph cycle that was essential in sequestering metal ions (Mn^{2+}, Fe^{2+}) from solution via enzymatic Mn(II) oxidation. Mn-oxide proto-ore was deposited in the sediment, serving as a paleoenvironmental indicator of oxic conditions. Cycle 2 was an anaerobic/suboxic heterotrophic bacterial cycle in which early diagenetic bacterially mediated Mn(IV) and Mn(III) reduction processes took place via organic matter oxidation and Mn-carbonate mineralization [2, 3]. For the source of metals low-temperature fluid flow along an associated fracture zone is preferred here [2].

The aim of the present study is to process and expand(?) the data collated during the longterm mining process. A greateraccuracy spatial image of the ore body can be obtained if the results gained from the processing of local data are taken into consideration. This, in turn, may impact on the understanding of essential genetic questions of the deposit and the potential for future exploration.

Field and drilling exploration of new mine fields are currently being undertaken within the Nyírszeg area (Fig. 1). Both the proposed new genetic model and re-evaluation of archive data may assist in answering questions, with the refinement of available genetical and structural models of new challenges and genetic questions which concern resource parameters.

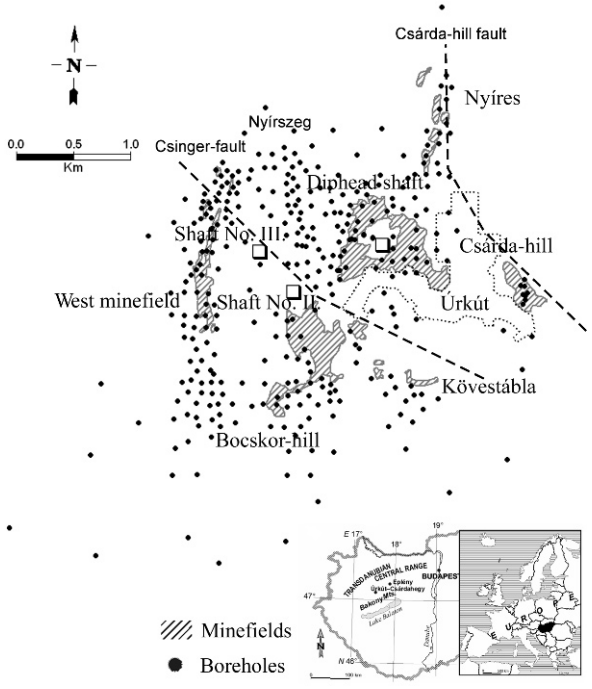

Figure 1. The minefields and the used boreholes in the Úrkút Basin

2. Geological setting

The Bakony Mountains of Hungary is an important region for structurally-controlled black-shale-hosted Mn-mineralization of Jurassic age. The Úrkút ore deposit (Úrkút Manganese Formation – ÚMnF) is located in the central part of the mountains, which belongs tectonically to the North Pannonian unit of the Alps-Carpathians-Pannonian region (Fig. 1; for more details see [4]). Nowadays, the economically important reserve covers around 8 km^2, with current reserves of 80 million tons of Mn-carbonate ore (24 weight percent average Mn and 10 weight percent Fe). The Mn-deposits occur within marine sedimentary rocks composed primarily of bioclastic limestone, radiolarian clay marlstone, and dark-grey to black shale [5].

From a tectonic point of view, there are two faults which have played an important role in the evolution of the area. The most important is the one which transects the Csárda-hill; a cca. 800 m long sinistral fault which was activated in the Jurassic, and its reactivation in the Cretaceous and in the Eocene resulted in horst and graben morphology. Another important structural line is the NW-SE Csinger-fault that transects the whole Úrkút Basin (Fig. 1).

Two distinct types of Mn-rich sedimentary rocks occur in the area, which represent relatively heterogeneous compositions and several sub-types. As all rock types (?) con-

tain elevated Mn concentrations, locally all varieties are referred to as ore. More detailed investigations will provide the discrimination between actual ore material and other Mn-rich rock types, as follows:

1. Cherty Fe-Mn-oxide mineralization occurs in multicolored metalliferous clays that overlie strongly leached and isolated Mn-impregnated limestone (Lower Liassic Hierlatz-type Limestone). The mineralization forms blocks, nodules and wad beds in close proximity to fracture zones oriented NNW-SSE along a mountain prominent structural trend ("Csárda-hill type ore"; Úrkút, Csárda-hill). At the Csárda-hill site, reworked detrital Mn-oxide ores may also occur [6]. As the borehole documentation does not separate different ore assemblages, the name for Mn-oxide ores of Csárda-hill in the current study will be referred to as fault-associated oxide ore (FAOx).

2. The second important ore type at the Úrkút deposit is black-shale-hosted Mn-carbonate ore that has formed due to bacterially mediated diagenetic processes [2, 3]. The carbonate ore type was recognized only in 1953 [2, 3]. The Mn-carbonate ore beds lie conformably on Middle Liass cherty limestone. Ore samples which have previously been described as Mn-carbonate in the borehole documentation may be subdivided into several subtypes (for more details see [2]). Proportions (?) of these Mn-carbonate ores later underwent *in situ* secondary oxidation and were partly reworked. Secondary oxidation of Mn-carbonate ore occurred along fault zones and tectonically elevated sections at later geological ages [6]. In this investigation, the two subtypes have not beendistinguished in the database. Therefore, the name "CAOx" carbonate-associated Mn-oxide ore has been applied.

The Csárda-hill mineralization in the Úrkút area has significance with respect to genetic studies of the Úrkút Mn-deposit, with the Csárda-hill mineralization differing from Mn-carbonate and CAOx, in that it is very cherty and Fe-rich, with the ore generally occurring in irregular depressions [2]. The FAOx was exploited in an open pit, with mining of this particular type of Mn-oxide ore being abandoned in the 1960s. The exploitation of Mn-carbonate ore increased only after 1996, once the Mn-oxide ore was depleted.

3. Methods

3.1. Data acquisition

The data used in this investigation was derived from a number of different sources. Research reports summarized by [1] contain information found in the archives of the operating company Mangán Ltd. Additional data was sourced from documentation of the Geological Institute of Hungary, while descriptions of boreholes in the databases of the Hungarian Geological Survey were also utilized.

Thetwo main sources of data provided boreholes (both surface and underground) and mine maps. The sources of data, their localities, the used methods and the purposes of analyses are summarized in Table 1.

The surface boreholes can be subdivided into two groups: deep boreholes – usually deeper than 100 meters (marked by U); and, shallow boreholes (marked by Cs, L, B, Kt and N). While the deep boreholes are available in a broad grid across the entire deposit area, shallow ones are available only in locations where the ore was near the surface, such as at Csárda-hill, Bocskor-hill, Kövestábla and the area of the Nyíres (Table 2A; Fig. 1; [7]).

Data acquisition and processing occurred separately for the different mine fields. In the first stage, only deep boreholes and underground mine data were acquired for four fields (shaft No. II. North-[Nyíres]; Diphead shaft; shaft No. III West; shaft No. II. South; Fig. 1). Underground boreholes (marked by UB) were used to ascertain the thickness of the deposit.

The results of mine mapping have been summarized in previous publications, in which both the underground boreholes and each characteristic stratigraphic level were evaluated [7]. In addition, the heading maps were scaled at 1:500 and in each case both sides of the mine tunnels were mapped. This information allows for the accurate representation of the the deformation of the deposit.

The chemical composition (with respect to Mn, Fe, Si, P) of 5,461 samples across the entire study area was also captured during this investigation (Table 2B). The chemical analytical data were acquired by wet chemical analyses in Laboratory of Úrkút Mine, Hungary. All analyses were carried out in the same laboratory and with the same analytical method. It may therefore be assumed that systematic measurement errors are unlikely to have occurred, and that the values will have similar reliability despite the fact that results represent several decades of analytical studies. The analytical error is estimated to not exceed ˜ 0.05 w/w% for the four components analyzed. To further test the consistency of the data, we analyzed the supervision also with statistical methods at the beginning of the study. The dataset was divided into two random populations of identical sizes and a two-sample f- and t-test

Table 1. The source and type of data, the purposes and the used methods for the different ore types.

Condition of database	Source of data	Type of data	References	Locality of ore types (Úrkút ore deposit)				Method	Purpose
				Proximal (Csárda-hill) (FAOx)		Distal (Úrkút basin)			
				Primary	Secondary	Primary	Secondary (CAOx)		
				Cherty, Fe-rich Mn-oxide ore	In situ altered and resedimented Mn-oxide ore	Early diagenetic Mn-carbonate ore	In situ altered and resedimented Mn-oxide ore (Nodular and laminated ore types)		
Raw data (summarized in borehole documentations and research reports)	1:500 scale level maps Σ 26 pieces	Coordinates	Orbán and Kohlrusz, 1973			✓	✓	Show in 3 D	3D model, heading maps demonstration
	1:500 scale level maps Σ 26 pieces	Types of tectonical movements				✓	✓	Stereographic projection	System of structural elements
	Samples from drillcores Σ 5.461 pieces	Chemical compositions of boreholes samples	Cseh Németh, 1960, 1963; Fekete and Cseh Németh, 1961; Szabó, 1965ab, 1966, 1970, 1973, 1980, 2006 Reports of boreholes' documentation Archive of Hungarian Geological Survey	✓ Σ 621 pieces		✓ Σ 266 pieces	✓ Σ 4.574 pieces	Uni- and multivariate statistics (correlational analyses, principal component analyses, discriminant analyses)	Examination of ore forming prosecces*
				✓ Σ 621 pieces		✓ Σ 266 pieces	✓ Σ 4.574 pieces	Uni- and multivariate statistics (correlational analyses, principal component analyses, discriminant analyses)	Classification of samples on their 4 element chemical composition
	Drillcore Σ 327 pieces	Boreholes		✓		✓	✓	Stochastic modelling (kriging)	3 D formation model, thickness maps
		Boreholes		✓				Correlational analyses, variogram surface	Statistical examination of chronostratigraphical levels, effect of tectonism**
		Boreholes				✓	✓	Stochastic modelling (kriging), univariate statistics, correlational analyses	3 D chronostratigraphical model, statistical examination of levels
		Boreholes				✓	✓	Compare of 3 D surface of formations	Examination of effect of tectonism (paleosurface recontruction)***

Notes: *The principal component (PC) analysis is such a statistical method which first aim is to reduce and summarize the data and it can show the independent processes. In the latter case during the principal component analysis process the relationships beetween each mutually connected variables are examined and these are showen on the basis of some interpreted principal components. Therefore it can determine the background process which influence the concentration of chemical components and it can classify the samples on the basis of these factors.

**Methods used for tectonical investigation: On the heading maps not only the observed lithological differences were noted, but the structural elements, too. The faults were drawn separately – without the shift, inclination angle and line of bearing – and the overlap faults, and anticline and syncline structures, and angular offset values determined in the heading belonging to the given rock type. These sequences could be illustrated – after the geocoding of the headings. Furthermore, the observed faults on the geological map sheets (Csima and Mészáros, 1976; Mészáros, 1976) could be comparing with the structural units of the illustrated sequences. Only the reverse faults could be evaluated in the observed structural elements along the headings, because the direction of the shifts of faults were not documented.

***Methods used for palaeosurface (relief) reconstruction: For this purpose that theory was followed that if the inclination angle map of the younger surface is extracted from the older surface's inclination angle map than with these extraction those tectonic effects disappear, which influenced both surfaces – namely those tectonic events which are more younger than the younger events. But those tectocic effects which happened between the age of the two palaeosurfaces, cannot be eliminated from the older surface, so the palaeosurface gives only approximately the original palaeosurface. The previous condition of the above evaluation is the missing of erosion, because the preservation of the tectonic effects can be preserved only in this case.

Table 2. A. The data of boreholes according to minefields. B. The data of samples according to boreholes.

Table 2A

Open pit	Period	Number of boreholes	Total length of boreholes (m)	Chemical analyses(No. of samples)
Csárda-hill	1957-61; 1970-72	88	1,209	758
Diphead shaft	1958-62	36	1,763	189
Bocskor-hill	1961-66	181	7,421	1,414
Kövestábla	1963-67	202	8,472	1,171
Nyíres	1978-80	38	1,642	493
Total *		*545*	*21,664*	*4,025*

Table 2B

Mine-field/drilling, sample (piece)	Shaft No. III. (W)		Diphead shaft		Shaft No. II., III.		Field Nyíres		Total5461
	U	UB	U	UB	U	UB	U	UB	
Drilling	38	62	32	64	6	16	33	85	327
Sample	765	432	0	413	34	45	609	633	2,931
Sample with oxide ore	251	358	0	101	5	11	324	261	1,311
Sample with carbonate ore	319	18	0	0	24	0	108	107	576

U: deep drilling
UB: drilling in the mine
* The difference between the two total values is because of boreholes out of open pits in case 2b.

were applied to identify whether the two groups belonged to the same population. At a 95% level of significance, the hypothesis that the two random groups had significantly different means for the above element was rejected. The results of the analyses may therefore be considered to be consistent, with any errors identified being due to random instrument/sample/human error. For a summary of the results, refer to Table 1.

In the early phase of the project it was important to build a database of the large number and wide spectrum of data. For this purpose, the coordinates of the surface and underground boreholes, the geochemical data, and the lithostratigraphic information were stored for each minefield. Each sample was assigned a unique identification code in order to make it possible to associate the element distribution and the results of statistical analysis with the boreholes, allowing the data to be represented spatially. The rule for creating unique identification codes for each sample was the following: sign and number of borehole, elevation above sea level (from-to), e.g. Cs-38_438.32-437.52. Along the boreholes the exact coordinates of the sequences were determined by trigonometric calculations, which were especially important in the case of the underground boreholes. Finally, as the result of the digitization process there are 30,934 individual data available for evaluation, including chemical analyses (Table 1).

3.2. Geomathematical methods

The available geochemical dataset was initially processed by univariate statistical analysis, to calculatethe essential descriptive parameters, including: mean, median, mode, standard deviation, range, minimum and maximum for each ore type independently. As the distributions for the elements studied were not normal, Spearman's rank correlation coefficient was calculated to determine the numerical relationship between the elements (?). To create a classification scheme of the samples based on their chemical compositions, different hierarchical cluster analyses were used, of which the Ward's method with squared Euclidean distance was found to be the most accurate. For objective evaluation of the result of the cluster analysis, discriminant function analysis was applied to quantify differences between the identified sample groups. For examination of the background processes that govern accumulation of chemical elements in the ores, principal component analysis was utilized. The series of maps of the resulting principal components which show spatial behaviour of the identified processes were found to bemore informative than the single element maps.

3.3. Geostatistical methods

A wide spectrum of maps were constructed using different processed borehole data for the whole Úrkút ore deposit, and some additional for important highlighted sub-areas (e.g. Csárda-hill; for details see Table 1). The aim of calculation and evaluation of the whole series of maps which concerned geochemical, stratigraphic, structural as well as topographic data was to be able to reconstruct evolution of the ore deposit in a spatial context. To get a reliable geological interpretation, each interpolated map

was evaluated using the digitized bedrock map. In case of the Csárda-hill area, a new bedrock map also had to be computed using the SE area borehole-depth dataset. In case of each thematic map, the applied interpolation method adopted was the ordinary kriging approach, for which variograms were fitted independently for single surfaces using Variowin [8]. To compute regional anisotropy, variogram surfaces were calculated and then used for mapping. Principal component maps which concentrate geochemical information were computed in the same way.

The resulting surfaces were used to construct dip-angle maps using the following equation [9]:

$$S_T = \frac{360}{2\pi} \arctan \left[\sqrt{\left(\frac{Z_E - Z_W}{2\Delta x} \right)^2 + \left(\frac{Z_N - Z_S}{2\Delta y} \right)^2} \right], \quad (1)$$

where: S_T = T point inclination angle

Z_E, Z_W = altitudes above sea level of points to the east and west from T point

Δx = distance between Z_E, Z_W

Z_N, Z_S = altitudes above sea level of points to the north and south from T point

Δy = distance between Z_N, Z_S

Dip-angle maps were used for paleo-relief reconstruction, so that extraction of neighbouring maps neglects tectonic effects younger than the age of the younger surface. Covariation of neighbouring surfaces was tested by correlation analysis.

The inverse faults indicated by the heading maps were plotted on a lower hemisphere stereographic plot, from which the direction of the compression event could be inferred.

4. Results

The first part of the results section reports on the evaluation of geochemical data of the main ore types (FAOx, CAOx and Mn-carbonate ores), extraction of background genetic processes using principal component analysis, as well as classification of the ores. The second part focuses more on maps of subsequent chronostratigraphic levels, altitude distributions and variogram surfaces, as well as tectonic considerations.

4.1. Evaluation of geochemical data

In the case of the FAOx sample group, all geochemical parameters studied exhibited a distribution far from normal. As a consequence, modes and the means were different, namely due to all elements having outlier concentrations, which significantly modified the means (Table 3A). To filter outlier values, box-plot diagrams were used (Fig. 2A). While the maximum values of Mn and Fe indicated excellent ore quality (Mn-ore, Fe-ore), those samples containing extremely low concentrations were defined as claystones. High Si-content (36.9 w/w% in average) indicated cherty and/or clayey material, while the distribution of P content in the ore washighly heterogeneous and did not show a clear tendency to accumulate in any well-defined ore type. Correlation analysis suggests significant relationships only between Mn and Si (-0.74, Table 4A).

The distribution of Mn concentrations in CAOx samples showed two modi (3.30 and 25.0 w/w%), i.e. the population of CAOx samples was subdivided into different types with different qualities (Table 3B). The maximum concentration of Fe indicated excellent iron ore quality, while those samples containing extremely low concentration were defined as claystones. High Si content (41.8 w/w%) indicated clay-rich formation with chert debris, whereas P usually

Table 3. The descriptive parameters of the elements.

A	FAOx sample set			
	Mn	Fe	Si	P
Mean	17.90	15.18	8.14	0.15
Median	17.23	15.43	8.95	0.16
Mode	18.40*	11.31*	1.50*	0.11
Relative deviation	0.53	0.35	0.68	1.21
Range	48.37	37.14	36.78	4.36
Minimum	0.10	2.23	0.19	0.02
Maximum	48.47	39.37	36.97	4.38

B	CAOx sample set			
	Mn	Fe	Si	P
Mean	17.12	10.87	13.90	0.18
Median	14.73	10.05	13.09	0.13
Mode	3.30*	8.10	3.51*	0.02
Relative deviation	0.73	0.42	0.59	1.56
Range	69.00	47.22	41.36	8.06
Minimum	0.00	0.98	0.49	0.00
Maximum	69.00	48.20	41.85	8.06

C	Manganese-carbonate sample set			
	Mn	Fe	Si	P
Mean	17.06	9.60	9.68	0.46
Median	16.34	9.21	9.14	0.41
Mode	17.99	6.70	5.94*	0.27
Relative deviation	0.46	0.45	0.49	0.71
Range	46.13	27.61	30.64	2.70
Minimum	0.96	0.73	0.98	0.05
Maximum	47.09	28.34	31.62	2.75

* Multiple modes exist. The smallest value is shown

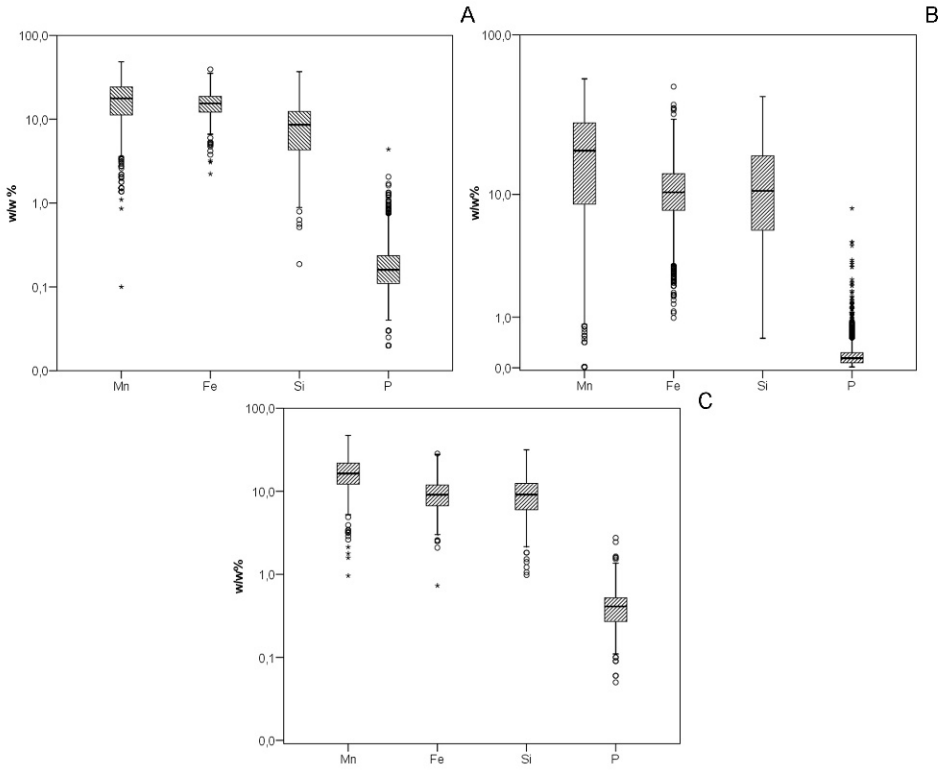

Figure 2. Box-plots of FAOx (A). The box-plot of CAOx sample set (B). The box-plot of Mn-carbonate sample set (C). Legend: the boxes show the distance between the lower and upper quartiles (above and below them 0.25 % and 0.75 % of the values can be found). The black line in the box is the median. The vertical lines show the 1.5 distance from quartiles values. Those values which are above or below this line are the outliers (o), and those, which are above or below the outliers are the extreme values (*).

occured in all ore types with a heterogeneous distribution. The wide range of concentrations and the outlier concentration values are shown on Fig. 2B. During the correlation analysis, the behavior of the elements was similar to that observed in case of the FAOx samples (Table 4B).

In the case of the Mn-carbonate group, the univariant parameters were similar to the above-mentioned ore types, although the weak negative Mn-Si correlation reported for the other ore types did not occur here (Table 4C).

Based on the result of the cluster analyses of FAOx, five sample groups were distinguished. As P was present sporadically and represented accumulation of fish fossils and phosphorite crusts (see Section xx), during sample classification only Mn, Fe and Si (elements significant for ore genesis) were included. Results of the classification were further studied by discriminant function analysis to test which elements were responsible for defining discrete sample groups. This approach confirmed that by chemical composition based grouping, 93.5 % of the samples were classified into the petrographically correct sample group. Summarizing the results, the following sample groups were distinguished (Fig. 3):

1. 1st group: clay with Mn-oxide, brown, red – multicolored – clay (lower Si-content) – 191 samples; Mn: 11.6 w/w% (median), min: 0.83 w/w%, max: 22.8 w/w%; Fe: 15.4 w/w%, min: 3.07 w/w%, max: 28.8 w/w%; Si: 12.1 w/w%, min: 1.59 w/w%, max: 22.8 w/w%.

2. 2nd group: clay with Mn-oxide, brown, red – multicolored – clay (higher Si-content) – 76 samples; Mn: 5.38 w/w% (median), min: 0.10 w/w%, max: 13.6 w/w%; Fe: 10.2 w/w%, min: 2.23 w/w%, max: 17.8 w/w%; Si: 20.1 w/w%, min: 14.0 w/w%, max: 37.0 w/w%.

3. 3rd group: Mn and iron oxide ore, brown, black, bluish-grey, hard oxide ore – 97 samples; Mn: 23.1 w/w% (median), min: 5.90 w/w%, max: 32.4 w/w%; Fe: 24.0 w/w%, min: 16.1 w/w%, max: 39.4 w/w%; Si: 2.80 w/w%, min: 0.63 w/w%, max: 9.13 w/w%.

4. 4th group: ferruginous Mn-oxide ore, and Mn-oxide ore, black, brown, red, yellow-multicolored Mn-oxide ore – 58 samples; Mn: 34.9 w/w% (median),

Table 4. The Spearman correlation matrix for the ores.

A	FAOx sample set			
	Mn	Fe	Si	P
Mn	1.00			
Fe	0.15	1.00		
Si	- 0.74	- 0.44	1.00	
P	0.13	-0.02*	- 0.12	1.00
B	**CAOx sample set**			
	Mn	Fe	Si	P
Mn	1.00			
Fe	0.01*	1.00		
Si	- 0.82	- 0.17	1.00	
P	0.20	- 0.02*	- 0.23	1.00
C	**Mn-carbonate sample set**			
	Mn	Fe	Si	P
Mn	1.00			
Fe	- 0.34	1.00		
Si	- 0.63	0.16	1.00	
P	- 0.16	0.29	- 0.12*	1.00

* Not significant ($\alpha = 0.01$)

min: 31.4 w/w%, max: 48.5 w/w%; Fe: 13.5 w/w%, min: 4.96 w/w%, max: 26.1 w/w%; Si: 2.87 w/w%, min: 0.19 w/w%, max: 8.65w/w%.

5. 5th group: clayey Mn ore, brown, red, yellow, multicolored, clastic, granular Mn-oxide-bearing clay – 198 samples; Mn: 21.2 w/w% (median), min: 14.8 w/w%, max: 31.7 w/w%; Fe: 15.2 w/w%, min: 6.98 w/w%, max: 22.9 w/w%; Si: 7.36 w/w%, min: 0.56 w/w%, max: 16.4 w/w%.

While a negative correlation occured between Mn-Si in the complete data set, in the case of the above groups, a weak negative correlation was determined between Fe-Si in the 2nd group (-0.66). High quality ores belonged to the 3rd, 4th and 5th groups (57% of samples), while the 1st and 2nd groups contained clay-rich manganiferous lithologies (43% of samples).

Based on cluster analyses of CAOx based on the three elements (Mn, Fe, Si,) five groups were distinguished. Here, 82.9% of the samples were classified into the proper petrographic cluster groups as follows (Fig. 4):

1. 1st group: Mn-bearing clay with Mn oxide and chert debris – 1,151 samples; Mn: 8.92 w/w% (median), min: 0.00 w/w%, max: 25.7 w/w%; Fe: 10.9 w/w%, min: 1.17 w/w%, max: 27.7 w/w%; Si: 17.5 w/w%, min: 2.08 w/w%, max: 30.9 w/w%.

2. 2nd group: layered, muddy Mn-oxide – 892 samples; Mn: 18.7 w/w% (median), min: 0.00 w/w%, max: 38.3 w/w%; Fe: 15.6 w/w%, min: 1.68 w/w%, max: 48.2 w/w%; Si: 8.90 w/w%, min: 0.61 w/w%, max: 23.0 w/w%.

3. 3rd group: layered Mn-oxide ore – 956 samples; Mn: 28.0 w/w% (median), min: 20.5 w/w%, max: 38.0 w/w%; Fe: 10.3 w/w%, min: 1.74 w/w%, max: 19.3 w/w%; Si: 7.15 w/w%, min: 0.56 w/w%, max: 17.2 w/w%.

4. 4th group: Mn-bearing clay with chert debris – 1,074 samples; Mn: 3.84 w/w% (median), min: 0.00 w/w%, max: 10.9 w/w%; Fe: 8.93 w/w%, min: 0.98 w/w%, max: 17.1 w/w%; Si: 23.7 w/w%, min: 18.4 w/w%, max: 41.9 w/w%.

5. 5th group: nodular, layered Mn-oxide ore – 500 samples; Mn: 39.7 w/w% (median), min: 30.8 w/w%, max: 69.0 w/w%, Fe: 6.98 w/w%, min: 1.40 w/w%, max: 20.8 w/w%, Si: 3.34 w/w%, min: 0.49 w/w%, max: 22.4 w/w%.

The highest quality Mn-oxide ores belonged to the 5th group, with an average Mn-content of ˜40 w/w%. Good quality ores belonged to the 2nd and 3rd groups, with a significant difference in Fe-content between them. The ore samples belonging to the 1st and 4th groups were Mn-bearing clays with chert debris.These ores did not contain less than 10 w/w% Mn. In summary, 51% of the evaluated samples belonged to good quality CAOx, while 49% belonged to Mn-bearing clays with chert debris.

Based on the classification of Mn-carbonate ores using the geochemical data (Mn, Fe, Si), five groups were distinguished, as follows (Fig. 5):

1. 1st group: Mn-bearing clay marlstone – 83 samples; Mn: 15.79 w/w% (median), min: 10.8 w/w%, max: 24.2 w/w%; Fe: 9.91 w/w%, min: 0.73 w/w%, max: 27.8 w/w%; Si: 10.3 w/w%, min: 2.76 w/w%, max: 16.2 w/w%.

2. 2nd group: clay-bearing Mn-carbonate, reflecting the average carbonate composition – 64 samples; Mn: 10.3 w/w% (median), min: 3.16 w/w%, max: 15.5 w/w%; Fe: 11.3 w/w%, min: 3.16 w/w%, max: 15.5 w/w%; Si: 11.3 w/w%, min: 4.19 w/w%, max: 16.9 w/w%.

3. 3rd group: high quality Mn-carbonate ore – 83 samples; Mn: 21.8 w/w% (median), min: 12.6 w/w%, max: 29.5 w/w%; Fe: 6.70 w/w%, min: 2.09 w/w%, max: 11.6 w/w%; Si: 6.08 w/w%, min: 0.98 w/w%, max: 13.5 w/w%.

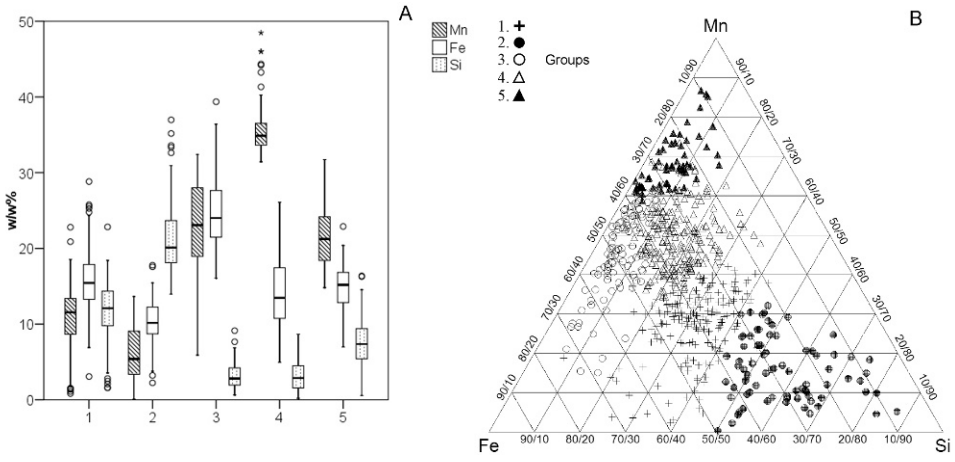

Figure 3. The box-plot (A) and Mn-Fe-Si diagram (B) of the received groups, FAOx sample set. Legend (all values are in w/w%): 1. group: clay with Mn-oxide, brown, red – varicoloured – clay (lower Si-content) – 191 samples; Mn: 11.55 (median), min: 0.83, max: 22.8, Fe: 15.4, min: 3.07, max: 28.8, Si: 12.1, min: 1.59, max: 22.8; 2. group: clay with Mn-oxide, brown, red – varicoloured – clay (higher Si-content) – 76 samples; Mn: 5.38 (median), min: 0.10, max: 13.6, Fe: 10.2, min: 2.23, max: 17.8, Si: 20.1, min: 14.0, max: 37.0; 3. group: Mn and iron oxide ore, brown, black, bluish-grey, hard, shatter fracture, oxide ore – 97 samples; Mn: 23.1 (median), min: 5.90, max: 32.4, Fe: 24.0, min: 16.1, max: 39.4, Si: 2.80, min: 0.63, max: 9.13; 4. group: ferruginous, Mn-oxide ore, and Mn-oxide ore, black, brown, red, yellow-varicoloured Mn-oxide ore – 58 samples; Mn: 34.9 (median), min: 31.4, max: 48.5, Fe: 13.5, min: 4.96, max: 26.1, Si: 2.87, min: 0.19, max: 8.65; 5. group: clayey Mn ore, brown, red, yellow, multicoloured, pea stonish, clastic, Mn-oxide-bearing granular clay – 198 samples; Mn: 21.2 (median), min: 14.8, max: 31.7, Fe: 15.2, min: 6.98, max: 22. 9, Si: 7.36, min: 0.56, max: 16.4.

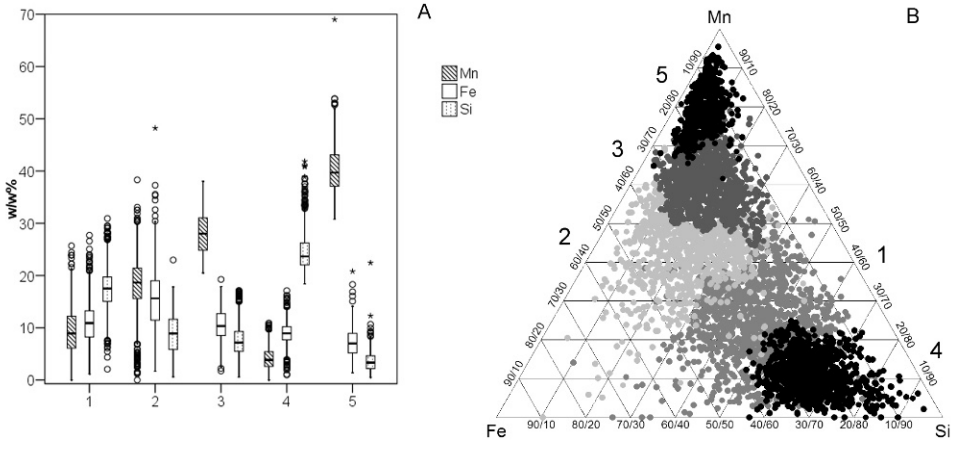

Figure 4. The box-plot (A) and Mn-Fe-Si diagram (B) of the received groups, CAOx sample set. Legend (all values are in w/w%): 1. group: Mn-bearing clay with Mn oxide and chert debris – 1,151 samples; Mn: 8.92 (median), min: 0.00, max: 25.7, Fe: 10.9, min: 1.17, max: 27.7, Si: 17.5, min: 2.08, max: 30.9; 2. group: layered, muddy Mn-oxide – 892 samples; Mn: 18.7 (median), min: 0.00, max: 38.3, Fe: 15.6, min: 1.68, max: 48.2, Si: 8.90, min: 0.61, max: 23.0; 3. group: layered Mn-oxide ore – 956 samples; Mn: 28.0 (median), min: 20.5, max: 38.0, Fe: 10.3, min: 1.74, max: 19.3, Si: 7.15, min: 0.56, max: 17.2; 4. group: Mn-bearing clay with chert debris – 1,074 samples; Mn: 3.84 (median), min: 0.00, max: 10.9, Fe: 8.93, min: 0.98, max: 17.1, Si: 23.7, min: 18.4, max: 41.9; 5. group: nodular, layered Mn-oxide ore – 500 samples; Mn: 39.7 (median), min: 30.8, max: 69.0, Fe: 6.98, min: 1.40, max: 20.8, Si: 3.34, min: 0.49, max: 22.4.

4. 4th group: Fe-bearing clay – 14 samples; Mn: 3.20 w/w% (median), min: 0.96 w/w%, max: 6.66 w/w%; Fe: 12.3 w/w%, min: 2.51 w/w%, max: 28.3 w/w%; Si: 19.0 w/w%, min: 9.91 w/w%, max: 31.6 w/w%.

5. 5th group: excellent quality ore (probably reflecting oxide zones in the carbonate ore) – 21 samples; Mn: 32.8 w/w% (median), min: 25.5 w/w%, max: 47.1 w/w%; Fe: 7.16 w/w%, min: 3.21 w/w%, max: 18.5 w/w%; Si: 5.52 w/w%, min: 2.29 w/w%, max: 8.80 w/w%.

In these groups, significant correlation existed between Fe and Si in the case of the 1st (-0.64) and the 4th (-0.63) groups (high Mn- and Fe-bearing clays).

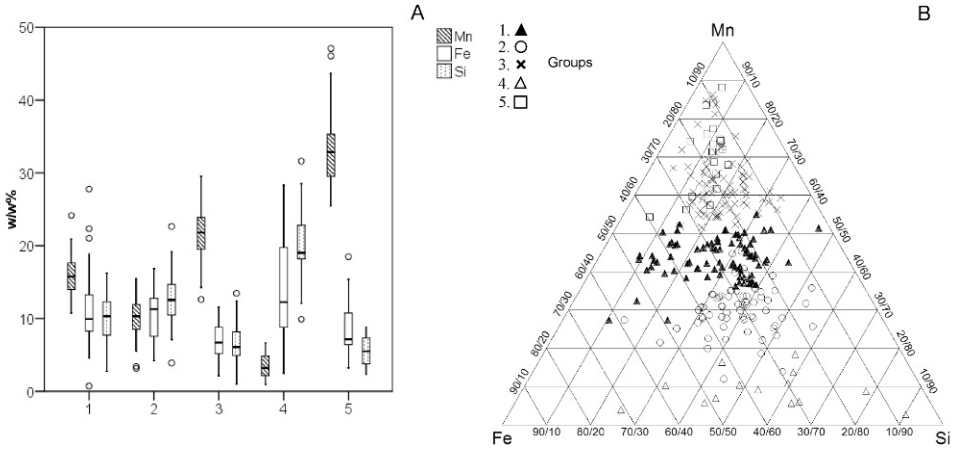

Figure 5. The box-plot (A) and Mn-Fe-Si diagram (B) of the received groups, Mn-carbonate sample set. Legend (all values are in w/w%): 1. group: higher Mn-bearing clay marlstone – 83 samples; Mn: 15.8 (median), min: 10.8, max: 24.2, Fe: 9.91, min: 0.73, max: 27.8, Si: 10.3, min: 2.76, max: 16.2; 2. group: clay-bearing Mn-carbonate, reflecting the average carbonate composition – 64 samples; Mn: 10.3 (median), min: 3.16, max: 15.5, Fe: 11.3, min: 3.16, max: 15.5, Si: 11.3, min: 4.19, max: 16.9; 3. group: excellent quality Mn-carbonate ore – 83 samples; Mn: 21.8 (median), min: 12.6, max: 29.5, Fe: 6.70, min: 2.09, max: 11.6, Si: 6.08, min: 0.98, max: 13.5; 4. group: high Fe-bearing clay – 14 samples; Mn: 3.20 (median), min: 0.96, max: 6.66, Fe: 12.3, min: 2.51, max: 28.3, Si: 19.0, min: 9.91, max: 31.6; 5. group: excellent quality ore (probably reflecting oxide zones in the carbonate ore) – 21 samples; Mn: 32.8 (median), min: 25.5, max: 47.1, Fe: 7.16, min: 3.21, max: 18.5, Si: 5.52, min: 2.29, max: 8.80.

To better understand the genetic circumstances of the three ore groups, principal component analyses were applied to FAOx, CAOx and Mn-carbonate sample groups. As accurate(?) results were obtained only in the case of the FAOx, results of the other two-ore types have not been presented. In case of FAOx, analysis resulted in three principal components (PC1–PC3) being determine which conclude the chemical parameters by the following measure (Table 5):

1. PC1 is associated with common increases of Mn and Fe and decrease of the Si-content (the values express relative strength).
2. In the case of PC2, Fe and P show contrasting behavior, i.e., the content of Fe decreases as the concentration of P increases.
3. PC3 is associated with attached enrichment of Fe and P.

All FAOx samples were classified into two large groups using cluster analysis based on the PCs. According to the box-plot diagram of the PCs (Figs 6AB) the two groups differed genetically from each other. The 1st group contained 81% of the total samples which were formed by the three processes in identical significance. In contrast, samples of the 2nd group (19% of the total samples) were mostly formed by PC1 (Fig. 6A). The 2nd group was subdivided into two subgroups (2A and 2B; Figs 6CD), which differed from each other in PC2 and PC3.

Table 5. The correlation matrix of the principal components and analyses.

	1st principal component	2nd principal component	3rd principal component
Mn	+ 0.8	+ 0.3	- 0.4
Fe	+ 0.6	- 0.5	+ 0.6
Si	- 0.9	- 0.2	- 0.1
P	- 0.2	+ 0.8	+ 0.5

4.2. Evaluation of spatial data

Histograms compiled from the altitude data of subsequent chronostratigraphic levels of the Úrkút Mn-deposit suggest that the recent surface relief is characterized by a negatively skewed distribution (Table 1, Fig. 7). In contrast, Jurassic and Cretaceous exhibited nearly symmetric, normal distributions. The altitude distributions of the footwall and hanging wall of the ore were similar (Fig. 8) suggesting an origin under comparable geologic circumstances, even if no linear correlation between the two surfaces ($r = 0.25$) was present. Generally, the ore body occured as small thickness stratiform sheets and did not infill deep basins. Nevertheless, in some places it becomes strikingly thicker, causing highly asymmetric distribution (Fig. 8).

When studying the relationship between subsequent surfaces (Table 6), the correlation between the recent terrain and the Eocene is visible. The Mesozoic levels do not

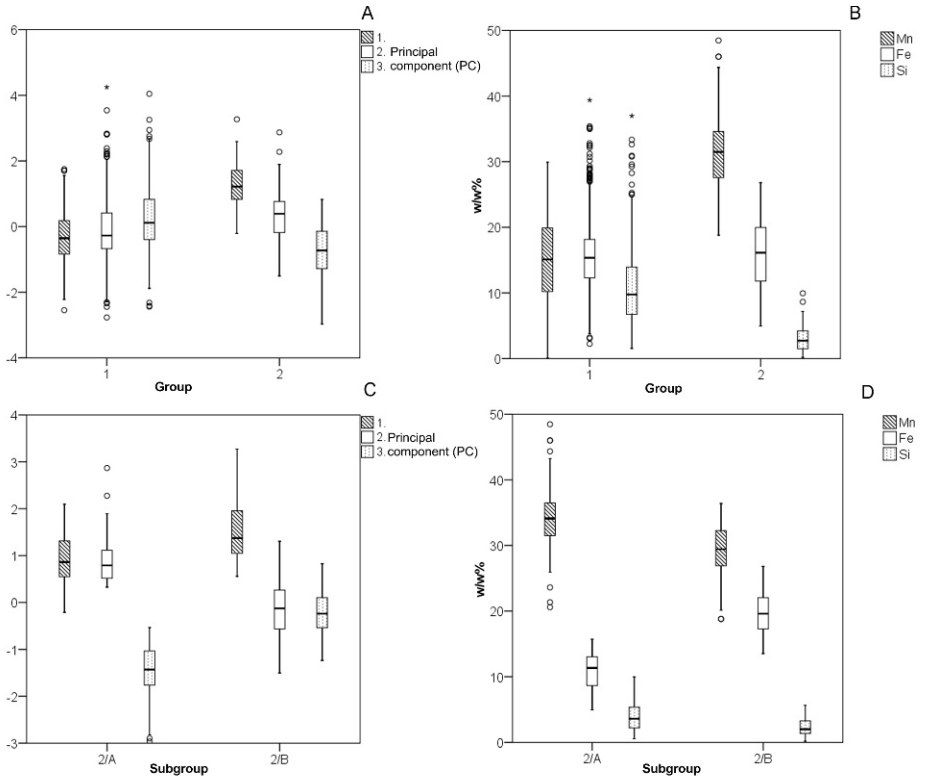

Figure 6. The strength of the groups of principal components (PCs) on box-plot diagram (A); the element concentration of the groups on box-plot diagram (B); the strength of the subgroups of 2nd group's principal components (PCs) on box-plot diagram (C); the element concentration of subgroups of the 2nd group on box-plot diagram (D).

Table 6. The correlation matrix of chronostratigraphical levels.

	Jurassic	Cretaceous	Eocene	Terrain
Jurassic	1.00			
Cretaceous	0.77	1.00		
Eocene	0.46	0.56	1.00	
Terrain	0.47	0.45	0.76	1.00

Table 7. Main tectonical direction and the rate of the anisotropy of the chronostratigraphical levels.

	Jurassic	Cretaceous	Eocene	Quarternary
Main direction	135-315°	125-305°	125-305°	165-345°
Anisotropy	1.8	2.7	1.4	1.3

correlate; insteadreflecting a possible impact of tectonic activity. The influence of these tectonic effects may also be tested by analyzing variogram surfaces for the chronostratigraphic levels. Calculations suggest that all surfaces are anisotropic and so can be characterized by the main tectonic directions (the big axis of anisotropy ellipse) and the degree of anisotropy (ratio of big and small axes) (Table 7).

In addition to a general evaluation of spatial data for the whole study area, a more detailed investigation was fulfilled in three smaller fields; Nyíres, Shaft III, W minefield and Csárda-hill in order to refine tectonic effects. Here, inclination angle maps were compiled using the relief model of FAOx and CAOx and the inclinational angle map of the footwall of the Albian limestone formation. The footwall of this limestone was primarily a clay marlstone, from which the development of the limestone was concordant. In the applied approach, the inclination angle map of the footwall of the Albian limestone was subtracted from the identical map of the Mn-oxide and, as a result, the inclination angle map of the Mn-oxide before the Albian was computed. In this way, the results of post-Albian tectonic effects were eliminated from both the relief model of the Albian limestone and Mn-oxide ore, as the pre-Albian effects did not affect the relief of the Albian limestone. For all three examined mine fields it was visible that the inclinational angle of the pre-Albian Mn-oxide ore relief varied around 10–20° (Fig. 9).

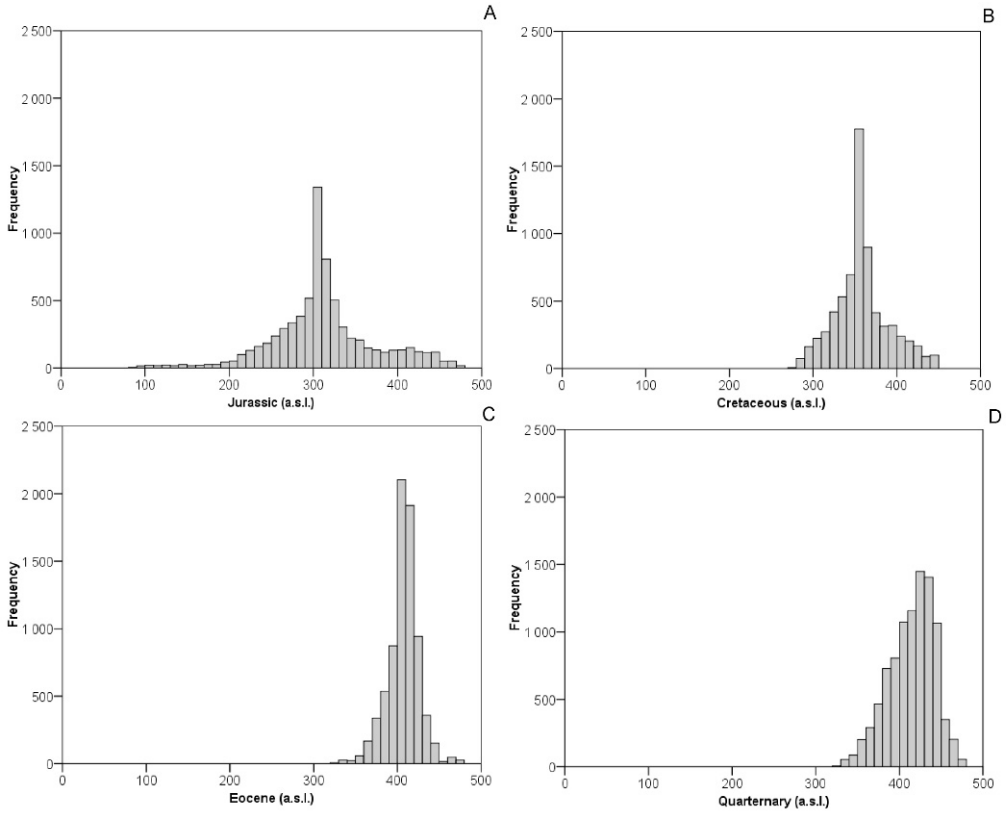

Figure 7. Histograms of the chronostratigraphical levels. Legend: a.s.l.: above (Baltic) sea level. (A) Jurassic; (B) Cretaceous; (C) Eocene; (D) Quarternary.

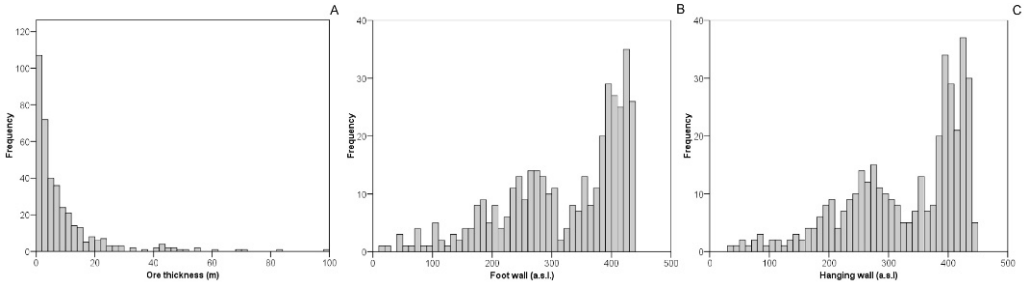

Figure 8. Histograms of drillings bound to the ore. Legend: a.s.l.: above (Baltic) sea level. (A) ore thickness; (B) footwall a.s.l.; (C) hanging wall a.s.l.

Reverse faults were documented primarily in shaft No. III W and Nyíres mine fields. In the central part of the deposit, reverse faults were unable to be defined. During the mapping at the Nyíres minefield, 62 faults were documented from which 22 were reverse faults, and one was a strike-slip fault (for the other faults no displacement was documented). By compiling only the reverse faults on the Angelier-type stereographical projection (lower hemisphere), it is obvious that they comprise one population (Figs 10AB). The interpretation of the reverse faults can be seen clearly on the reconstructed stress field ("beach ball"). According to this approach, the reverse faults of the Nyíres minefield are the effect of an E-W compression activity. Observations in the shaft No. III, W-minefield lead to similar conclusions, where 68 structural units (faults) were documented as a total, from which 22 were reverse faults (Figs 10CD). As a consequence, assuming a deposition on a flat surface of the overlying Albian limestone, this compression may be associated with the Aptian-Albian

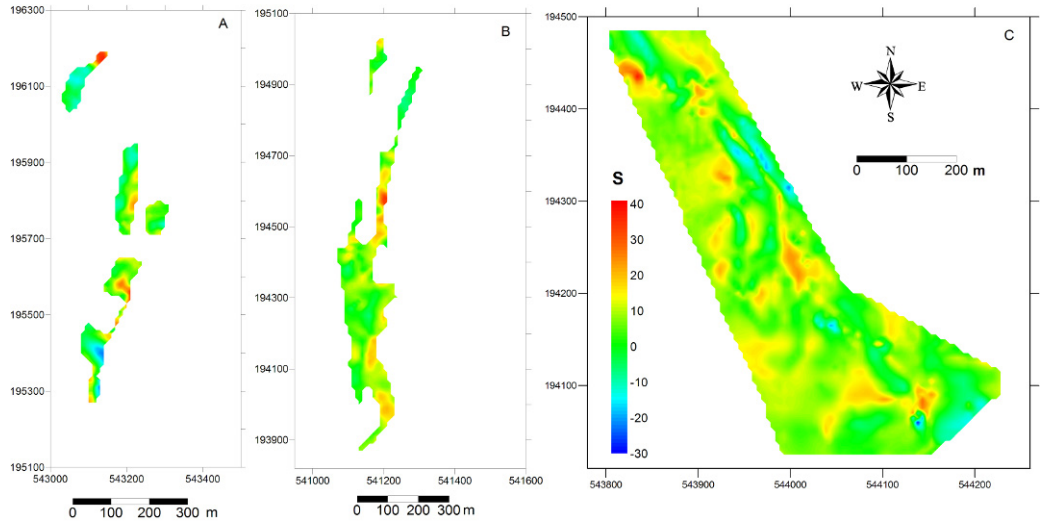

Figure 9. The Nyíres minefield (A) and the shaft No. III, western part's (B) Mn-oxide ore structured angle's (S) map with the tectonical elements (0° is horizontal), (C) the map of the hanging wall's and the footwall's angle difference in Csárda-hill.

border, which may have also caused intense folding of the Mn-bearing strata [10].

5. Discussion

5.1. Ore types, spatial relationship

The results of statistical evaluation of geochemical data show that the historical information available for different ore types reflect heterogeneous compositions changing from different quality ore types to manganiferous clays and claystones. The elements are correlated weakly with each other, likely due to one or more syngenetic or postgenetic processes. Principal component analysis reveals these fundamental processes. The first of these (PC1), is thought to reflect the same source for Mn and Fe. Among others, these attributes are characteristic for hydrothermal systems where ore forming processes move Mn and Fe together [11–19]. Previous studies also raised this for Úrkút Mn-deposit [20–25]. A hydrothermal/exhalative source of metals may have contributed to the formation of the deposits. A Fe-Mn-oxide chimney system is proposed to have been a proximal facies to geofluid vents that occurred along fracture systems, which may have provided metals from deep-seated sources [2]. Evidenceof microbial contribution (stromatolite-like structures, clumps of bacteria, etc.) and detailed geochemical studies, showed element ratios (Si/Al, Mn/Fe, Al/Al+Fe+Mn).Interpretation on a smaller set of samples supported the evidences of hydrothermal contribution [2]. Recent studies also arrived at the same solution, providing further eevidence.

In submarine hydrothermal mixing zones, Fe precipitates very quickly to an oxide by autocatalytic processes [26], with Fe-oxide providing an active surface to precipitate Mn (active oxide surface precipitation model, [27]). This could be the case at the Csárda-hill area Fe-Mn oxide chimney system [2]. In the case of PC2, Fe and P co-vary systematically. This is attributed to the enrichment of the primary sediment with organic matter, as evidenced by an abundance of fish and other fossils that are responsible for the local enrichment of P, caused by intense bacterial/algal organic matter accumulation [25, 28]. Finally, PC3 is explained by the effect that would reflect the similar attitude and relative enrichment of Fe and P, or absorption of P on an active surface of Fe-oxi-hydroxide in a submarine environment.

When studying spatial distribution of these processes, the key question is to analyze the principal component and element concentration maps around the deep depressions. These submarine dissolved surfaces could be the sites where via leaching of the underlying limestone multicoloured metalliferous clay (umber, ochre) and cherty Fe-Mn oxide mineralization took place synchronously [2]. In this sense, these depressions could be the feeder channels of hydrothermal, geofluid discharge to seawater: the source of the metals. That is why it was important to elaborate the element distribution along these depressions in vertical and horizontal directions to show whether the metalliferous assemblages are primary accumulations or

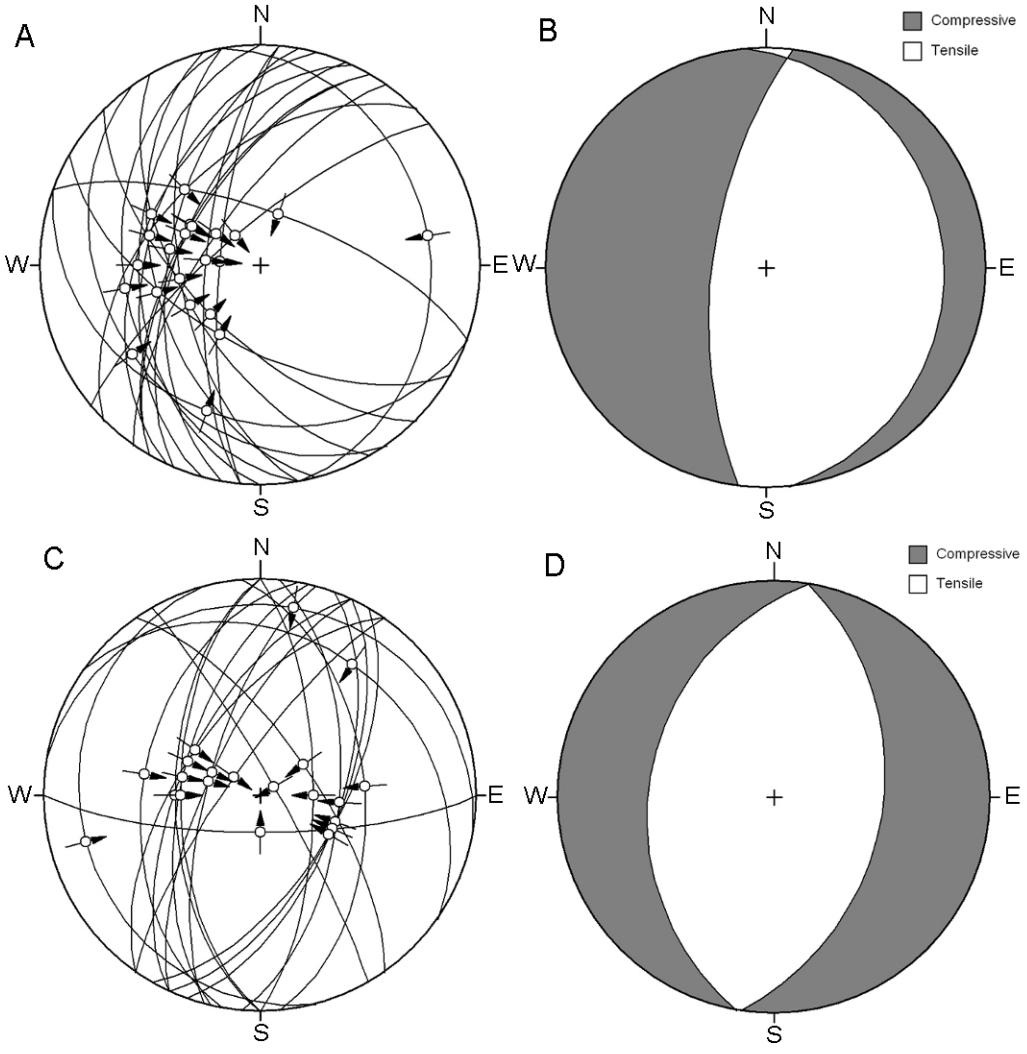

Figure 10. The Nyíres minefield reversed faults: (A) stereographical projection and the reconstructed (B) stress field, shaft No. III, W- minefield's reversed faults' (C) stereographical projection and the reconstructed (D) stress field.

supergene resedimented successions. Concerning Fe and Mn, increases are observed in the southern part of the study area surrounding the 3rd and 4th depression, while around the 1st and 2nd depressions the Mn, Fe distributions in vertical direction are nuanced. The same spatial pattern is observed on the principal component maps. The effect of PC1 (Mn and Fe move together) is the strongest along the depressions, generally on the western side of the study field (Fig. 11). Organic matter in the primary sediment (PC2) is homogeneously distributed throughout the area. A less important enrichment in PC2 in the southern part likely developed due to the occurrence of Mn-carbonate ore and its higher P content. The considerable amount of fish debris (P-rich) can be interpreted as an indirect evidence of high bacterial/algal organic productivity [2]. The PC3 map displays two maxima, with both near to the southern depressions. Nevertheless, the average value of PC3 is high in the whole area, suggesting a notable effect.

For the Csárda-hill area (oxide ores), principal component analysis resulted in three main processes which were used to provide a more detailed sample classification scheme. The two main groups defined showed significant differences in Fe and Mn concentrations (Fig. 6B). In the 2nd group, the high quality Mn-ores belonged to the 2A subgroup (Fig. 6D), while in the 2B subgroup the Fe concentration showed concentrations of up to 20 w/w%. On PC maps, subgroup 2A samples infilled the depressions and occured directly around them, while the samples

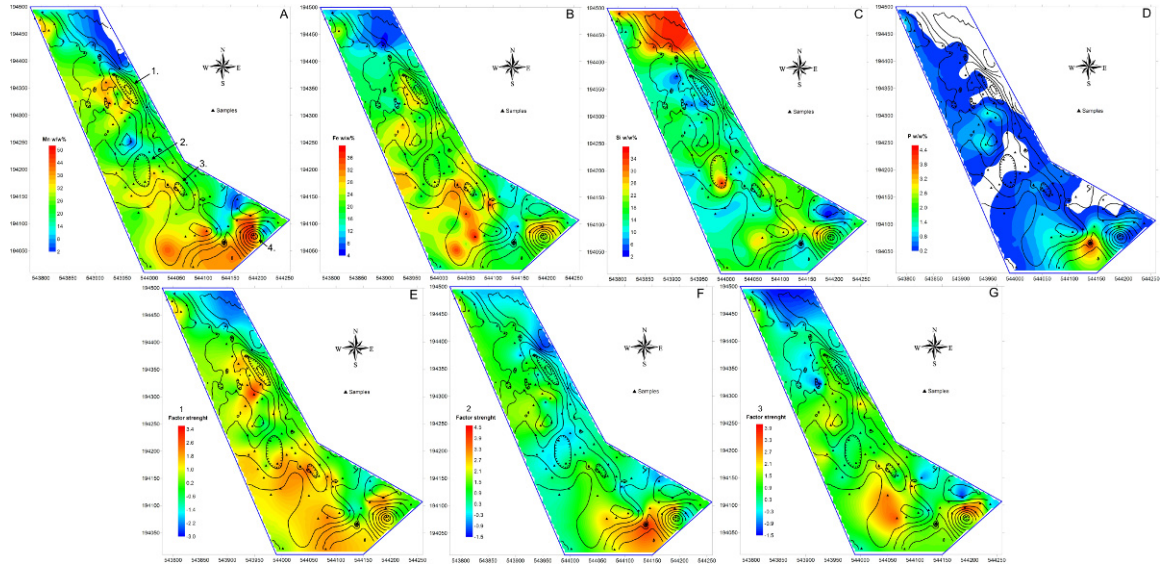

Figure 11. The spatial distribution of maximum values of elements on Csárda-hill (A) Mn, (B) Fe, (C) Si, (D) P and distribution of principal components (E) 1st PC, (F) 2nd PC, (G) 3rd PC. The numbers show the topography of the footwall depressions, the contour interval 5 m.

of group 2B appeared more spread out across the field (Fig. 11).

5.2. Stratigraphy, tectonic evolution

Geostatistical investigations of the chronostratigraphic levels provide an even greater comprehensive picture of basin evolution. Interpolating with variogram-based kriging of each level, it can be seen that the ranges of variograms of single levels differ from each other. Younger levels have greater levels, while older levels have smaller ranges. Younger strata have less articulate surfaces than the older strata, suggesting that the deformation effects decline towards younger formations. The most essential formation effect is considered to be the tectonic movements (i.e. the process of fault driven block formation), and Aptial-Albian intense local folding. Similar conclusions may be drawn from the correlation coefficients between the values of the elevations above sea level of the constructed chronostratigraphic surfaces.

The correlation matrices calculated from the elevation points of the surfaces show the linear similarity between them. Surfaces do not correlate with the recent relief, but the correlation coefficients with the present-day surface increase towards younger strata. Consequently, the Mesozoic levels are less similar than the Eocene surfaces. That is, the older the level, the less its similarity with the recent relief (rock types are similar, limestones). This may possibly be a result of tectonic activity, since the present-day relief is governed by erosion and not by tectonics.

Consequently, the results of the two different methods are similar, and logically conform toeach other, while they are not in conflict with the known regional tectonic model. While different brittle and compression episodes controlled the build-up in the Mesozoic (formation of platforms in the Triassic, their blocking in the Jurassic, and compression in the Cretaceous), in the Tertiary less articulate platforms formed, and the effect of erosion marked the Quaternary [10].

The histograms showing elevation above sea level of the footwall and hanging wall relief models are similar, resulting from tectonic processes. If the two histograms display similar distributions, then they are likely to have been produced by similar effects; that is, no tectonic event occurred during the time of deposition. This implies that during formation of the ore there was no synsedimentary tectonic effect. This is not in conflict with the known evolution scheme, since it is rather possible during the short term of ore formation as previously suggested [28].

In the case of the Csárda-hill, the low value of the correlation coefficient suggests that the footwall and the hanging wall relief models are not similar. Erosion of the overburden may have had a greater effect than tectonics, since a tectonic effect – as mentioned above – should be manifested in both surfaces. Depressions of the footwall should come to end before the formation of the covers, otherwise similar depressions should be present in the hanging wall. Variograms of both the footwall and the hanging wall, calculated based on their elevation values, displayed the same anisotropy. This concurs with the trend of the 800 m

dextral strike-slip fault, thus possibly the depressions of the footwall are a result of tectonic preformation.

Inverse faults exposed by the headings imply E-W compression. This compression is present at headings of both mining sites, both at the western field and the Kislőd field at the northern part of the basin. The E-W compression was extant in the Middle Cretaceous during the structural development of the Transdanubian Mountains, and the southern Bakony Mountains [10]. This direction concurs with that of the compression that formed anticlines and synclines in the basin.

The palaeo-relief studies gave similar results for both areas (shaft No. III, western field, Nyíres-Kislőd field). These suggest that the dip of the strata of the Lias Mn ore is no more than 10-20°. Such aflat topography is in accordance with the relief suggested by previous genetic models, which interpreted the formation of the ore on a seafloor. Since there is no dominant direction on the constructed paleo-relief map, the resulting directions of the former tectonic studies are likely to be attributed toan effect of tectonics.

6. Conclusion

During the review of Úrkút Mn deposit, over 30,000 single historical data were digitized, covering a wide spectrum of information. The most important results of the re-evaluation of this large dataset can be summarized as follows:

1. During the Mn-carbonate ore formation the sea floor was a smooth surface with 10-20° dip angle, based on the results of palaeo-topographic reconstruction.

2. Formation of the oxidized Mn ore wasa result of two processes based on the geomathematical analysis of FAOx. The most important effect was the hydrothermal process (PC1) which enriched Mn and Fe together nearby to the depressions. The other significant effect (PC2: primary sediment) was most effective at the central part of the Csárda-hill area.

3. Upper Liass Mn-carbonate ore formation – which was a short time event – was undisturbed by synsedimentary tectonic effects due to the influence of tectonic activity which was unable to be detected between the hanging wall and footwall layers.

4. The observed intensive folding of Mn-carbonate ore was caused by E-W compression effects in the Lower Cretaceous (at the border of Aptian-Albian).

Acknowledgements

The authors thank Zoltán Szabó Ph.D. (Mangán Ltd. Úrkút) for the helpful contributions and advice. The authors are also grateful to Sarolta Bodor Ph.D. student for data capturing, József Kovács Ph.D. for his help in the initial steps and to József Knauer Ph.D. for classification of boreholes to formations. The authors thank Prof. Jens Gutzmer for useful comments. The study was supported by the grant of Pro Renovanda Cultura Hungariae "Students for Science", and by the Hungarian Science Foundation (OTKA-NKTH No. K 68992).

References

[1] Bíró L., Polgári M., Tóth T., Kovács J., Knauer J., Vigh T., Reappraisal of archive data of manganese ore (Úrkút, Hungary) (in Hungarian). GeoLitera Publisher, Szeged, Hungary, 2009

[2] Polgári M., Hein J.R., Vigh T., Szabó-Drubina M., Fórizs I., Bíró L., Müller A., Tóth A.L., Microbial processes and the origin of the Úrkút manganese deposit, Hungary. *Ore Geol. Rev.*, 2012, doi: 10.1016/j.oregeorev.2011.10.001.

[3] Polgári M., Okita P.M,. Hein J.R., Stable Isotope Evidence for the Origin of the Úrkút Manganese Ore Deposit, Hungary. *J Sediment. Petrol.,* 1991, 61, 384-393

[4] Haas J., Influence of global, regional, and local factors on the genesis of the Jurassic manganese ore formation in the Transdanubian Range, Hungary. *Ore Geol. Rev.,* 2012, doi:10.1016/j.oregeorev.2011.08.006

[5] Polgári M., Manganese geochemistry reflected by black shale formation and diagenetic processes - Model of formation of the carbonatic manganese ore of Úrkút: Special Series of Hungarian Geological Institute, Karpati Publish House, Ushgorod, 1993

[6] Cseh Németh J,. Grasselly G., Szabó Z., Sedimentary manganese deposits of Hungary. In: Varentsov I,M,, Grasselly G. (Eds), Geology and Geochemistry of Manganese. Akadémiai Kiadó (Budapest) 1980, 2, 199-223

[7] Szabó Z., Mining of manganese in Bakony mountains. In commemoration of mining engineer József Farkas. Mangán Ltd. Úrkút, Ajka, 2006

[8] Variowin P.Y., Software for Spatial Data Analysis in 2D. Springer Verlag, 1996

[9] Moore I.D., Lewis A., Gallant J.C., Terrain properties: Estimation Methods and Scale Effects. Modeling Change in Environmental Systems. John Wiley and Sons, New York, 1993

[10] Haas J., Geology of Hungary. Eötvös Lorand University Publishing House, Budapest, 2001

[11] Boström K., Kraemer T., Gartner S., Provenance and accumulation rates of opaline silica Al, Ti, Fe, Mn, Cu, Ni and Co in pelagic sediments. *Chem. Geol.*. 1973, 11, 123-148

[12] Bonatti E., Zerbi M., Kay R., Rydell H., Metalliferous deposits from the Apennine ophiolites: Mesozoic equivalents of modern deposits from oceanic spreading centers. *Geol. Soc. Am. Bull.*, 1976, 87, 83-94

[13] Crerar D.A., Namson J., Chyi M.S., Williams L., Feigenson M.D., Manganiferous cherts of the Franciscan assemblage: I. General geology, ancient and modern analogues, and implications for hydrothermal convection at oceanic spreading centers. *Econ. Geol.*, 1982, 77, 519-540

[14] Bonatti E., Hydrothermal metal deposits from the oceanic rifts: a classification. In: Rona P.A., Bostrom K., Laubier L., Smith Jr. K.L. (Eds.), Hydrothermal processes at seafloor spreading centers. New York, Plemun Press 1983, 595-663

[15] Robertson A.H.F., Boyle J.F., Tectonic setting and origin of metalliferous sediments in the Mesozoic Tethys ocean. In: Rona P.A., Bostrom K., Laubier L., Smith Jr. K.L. (Eds.), Hydrothermal processes at seafloor spreading centers. New York, Plemun Press 1983, 595-663

[16] Glasby G.P., Hydrothermal manganese deposits in island arcs and related to subduction processes: a possible model for genesis. *Ore Geol. Rev.,* 1988, 4, 145–153

[17] Chen J.C., Owen R.M., The hydrothermal component in ferromanganese nodules from the sutheast Pacific Ocean. *Geochim. Cosmochim. Ac.*, 1989, 53, 1299-1305

[18] Hein J.R., Koschinsky A., Halbach P., Manheim F.T., Bau M., Kang J.K., Lubick N., Iron and manganese oxide mineralization in the Pacific. Manganese mineralization: geochemistry and mineralogy of terrestrial and marine deposits. Geological Society Special Publication, London, 1997, 119, 123–138

[19] Nath B.N., Plüger W.L., Roelandts I., Geochemical constraints on the hydrothermal origin of ferromanganese encrustations from the Rodrigez Triple Junction, placeIndian Ocean. In: Manganese Mineralization: Geochemistry and Mineralogy of Terrestial and Marine Deposits. Geological Society Special Publication, London, 1997, 199-213

[20] Szabó Z., The genesis of the manganese deposits, Bakony Mts. Ph.D. Thesis, József Attila University, Szeged, Hungary, 1977

[21] Szabó Z., Grasselly G., Genesis of manganese oxide ore in the Úrkút basin, Hungary. In: Varentsov I.M., Grasselly G. (Eds.), Geology and Geochemistry of Manganese. Akadémiai Kiadó (Budapest) 1980, 2, 223-236

[22] Szabó Z., Grasselly G., Cseh Németh J., Some conceptual questions regarding the origin of manganese in the Úrkút Deposit, Hungary. *Chem. Geol.,* 1981, 34, 19-29

[23] Kaeding L., Brockamp O., Harder H., Submarin-Hydrothermale Entstehung der Sedimentaren Mn-Lagerstatte Úrkút (Ungarn). *Chem. Geol.,* 1983, 40, 251-268

[24] Varentsov I.M., Grasselly G., Szabó Z., Ore-formation in the early-Jurassic basin of Central Europe: Aspects of mineralogy, geochemistry and genesis of the Úrkút manganese deposit, Hungary. *Chemie der Erde,* 1988, 48, 257-304

[25] Polgári M., Szabó-Drubina M., Szabó Z., Theoretical model for the Mid-European Jurassic Mn-carbonate mineralization Úrkút, Hungary. *Bulletin of Geosciences*, 2004, 79, 53-61

[26] Humphris S.E., Zierenberg R.A., Mullineaux L.S., Thomson R.E. (Eds), Seafloor hydrothermal systems. Physical, chemical, biological, and geological interactions. American Geophysical Union, Washington DC. USA, 1995

[27] Morgan J.J., Kinetics of reaction between O_2 an Mn(II) species in aqueous solutions. *Geochim. Cosmochim. Ac.*, 2005, 69, 35-48

[28] Polgári M, Szabó Z, Szederkényi T. (Eds). Manganese Ores in Hungary. Regional Committee of the Hungarian Academy of Sciences, Szeged, Juhász Publishing House, 2000